Dalton Transactions

ROYAL SOCIETY OF CHEMISTRY

PAPER

View Article Online
View Journal | View Issue

Check for updates

Cite this: *Dalton Trans.*, 2025, **54**, 11533

An $Eu_4L^4{}_4$ tetrahedron with multiple recognition sites: a luminescent sensor for rapid and sensitive detection of biogenic amines†

Yuan Yao,[a] Li Li,[a] Tongxi Zhou,[a] Su Wang,[a] Ying Qin,[a] Chao Fan,[a] Yuying Fu,[a] Guoliang Liu*[a] and Hongfeng Li*[b]

Biogenic amines are important bioactive substances in living organisms, and their abnormal metabolism can serve as biomarkers for certain diseases such as depression, Parkinson's disease and transient tic disorder. Therefore, developing a highly efficient and sensitive luminescent sensor for biogenic amines is essential. However, the biological system is a complex liquid environment containing multiple active substances, which can reduce effective collisions between the sensor and the target analyte, thereby diminishing the sensor's sensitivity. To address this issue, we introduced reaction sites that can undergo nucleophilic and hydrogen bonding interactions with amino groups into the structure of the sensor, and designed and synthesized a multi-site tetrahedral cage $\mathbf{Eu_4L^4{}_4}$ to achieve specific capture of biogenic amines. By leveraging these dual interactions between $\mathbf{Eu_4L^4{}_4}$ and amines, combined with the confined cavity effect of the cage, multiple spectroscopic analyses demonstrated that the detection limit for ethylenediamine (EDA) improved from 370 μM ($\mathbf{Eu_4L^1{}_4}$) to 33 μM ($\mathbf{Eu_4L^4{}_4}$), while the response time decreased from 1.1 seconds to 0.81 seconds. This design provides an effective strategy for enhancing sensor sensitivity and paves the way for its application in detecting biogenic amines within biological systems.

Received 25th March 2025,
Accepted 30th June 2025

DOI: 10.1039/d5dt00720h

rsc.li/dalton

1. Introduction

Biogenic amines (BAs) are a group of biologically active amine compounds widely present in living organisms.[1] Among them, diamines are the most common, including cadaverine, putrescine, histamine, tyramine, spermine, and spermidine.[2] Trace amounts of biogenic amines are normal active components in living organisms and play important physiological roles in biological cells. However, abnormal amounts of biogenic amines are associated with cell division and have been reported as biomarkers for human diseases, such as depression, Parkinson's disease and transient tic disorder.[3] Therefore, it is essential to develop a biogenic amine sensor capable of detecting these compounds in biological systems.

Currently, various analytical methods for evaluating biogenic amines have been reported, including electrochemical analysis (EC),[4] capillary electrophoresis (CE),[5] high-performance liquid chromatography (HPLC),[6] and gas chromatography (GC) methods.[7] However, these methods are often limited in practical applications due to their reliance on expensive instruments, complex sample pretreatment procedures, and cumbersome operations.[8] In contrast, fluorescence sensors offer significant advantages, such as low cost, simple operation, rapid response time, high sensitivity and high selectivity.[9] As a type of fluorescent sensor, lanthanide-based sensors have attracted increasing attention due to their high sensitivity, offering advantages such as high luminescence quantum yields, long luminescence lifetimes, and large Stokes shifts.[10] Their long luminescence lifetimes enable lanthanide sensors to distinguish their signals from interfering background fluorescence in complex biological systems.[11] These sensors have been widely used for the detection of biogenic amines,[12] metal ions,[13] anions,[14] biomolecules,[15] and amino acids[16] in biological systems.

However, living organisms represent complex solution environments where numerous coexisting biomolecules with similar functional groups compete with the target analyte. This complexity significantly reduces the effective collisions between the sensor and the analyte, leading to poor selectivity and even erroneous signals. These drawbacks greatly compromise detection accuracy. In recent years, to improve selectivity

[a]College of Sports Science and Health, College of Sports Science Research, Harbin Sport University, Harbin 150008, Heilongjiang, People's Republic of China. E-mail: lgl1800@163.com
[b]School of Chemistry and Materials Science, Key Laboratory of Functional Inorganic Material Chemistry, Ministry of Education Heilongjiang University, 74 Xuefu Road, Harbin 150080, China. E-mail: lihongfeng@hlju.edu.cn

† Electronic supplementary information (ESI) available. See DOI: https://doi.org/10.1039/d5dt00720h

and sensitivity, some sensors with increased reaction sites have been reported.[17] When the analyte is added, the sensor with a specific functional group can recognize the analyte through covalent or non-covalent interactions. Once multiple recognition sites are introduced into the structure of the sensor, the interactions between the sensor and the target analytes will be enhanced, effectively improving the sensitivity and selectivity of the sensor.[18]

Herein, a discrete tetrahedral cage, $\mathbf{Eu_4L^4{}_4}$, with multiple recognition sites is designed based on a tris-β-diketone ligand ($\mathbf{L^1}$). In previous studies, we confirmed that weak intermolecular nucleophilic interactions between β-diketones and analytes containing amino groups can occur in $\mathbf{Eu_4L^1{}_4}$, $\mathbf{Eu_4L^2{}_4}$, and $\mathbf{Yb_4L^3{}_4}$ films at room temperature[19] (the structures of ligands $\mathbf{L^1}$, $\mathbf{L^2}$, and $\mathbf{L^3}$ are shown in Fig. S1†). However, this weak nucleophilic effect is significantly diminished in the liquid state. To address this issue, $\mathbf{Eu_4L^4{}_4}$ is designed with multiple pyridine sites on the cage's skeleton, which can interact with analytes *via* weak intermolecular nucleophilic interactions and hydrogen bonding. Additionally, the confined environment of the tetrahedral cavity may selectively accommodate target molecules of a specific size, further enhancing the sensor's selectivity. Based on a series of sensing performance tests, the detection limit of $\mathbf{Eu_4L^4{}_4}$ for ethylenediamine (EDA) is reduced from 370 μM ($\mathbf{Eu_4L^1{}_4}$) to 33 μM. This improvement demonstrates that introducing multiple reactive sites into the sensor significantly enhances its sensitivity. In summary, the design of a tetrahedral cage with multiple reactive sites provides a new strategy for improving the sensitivity and selectivity of sensors in complex biological systems (Chart 1).

2. Results and discussion

2.1 Synthesis and characterization

The ligand synthesis follows a four-step process outlined in Scheme 1 (details in the ESI†). The first step involves the copper-catalyzed Ullmann coupling of 3-methoxyaniline with 1-iodo-3-methoxybenzene to form 3,3′,3″-trimethoxytriphenylamine (**TTA**). In the second step, Friedel–Crafts acylation is employed to synthesize 3,3′,3″-trihydroxy-4,4′,4″-triacetyltrianiline (**TTTA**). The third step involves the Ullmann reaction of **TTTA** with trichloromethylpyridine hydrochloride, yielding tri

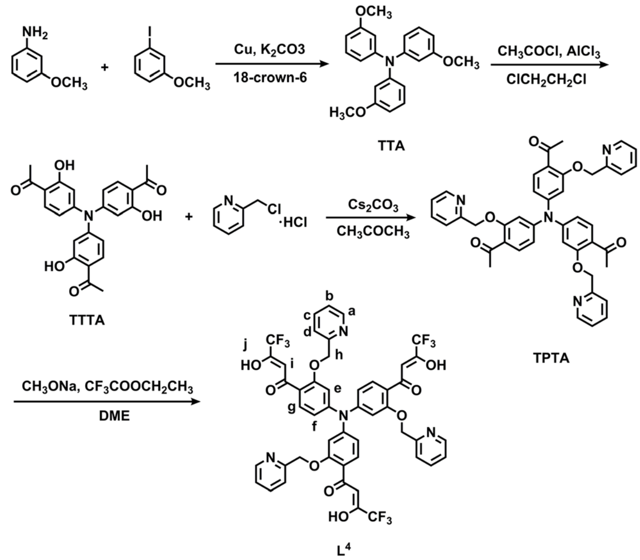

Scheme 1 The synthetic pathway for $\mathbf{L^4}$.

(3-(2-)pyridyl methoxy)-tri(4-acetyl)triphenylamine (**TPTA**). Finally, a Claisen condensation between **TPTA** and ethyl trifluoroacetate produces the target ligand $\mathbf{L^4}$. The successful synthesis of the ligand and its intermediates was confirmed using ^{1}H NMR and ESI-TOF-MS (Fig. S2–S11†).

The ligand was then reacted with the corresponding Ln(III) salts in a methanol solution at a 1 : 1 stoichiometric ratio for 24 hours to form a lanthanide tetrahedron. ESI-TOF-MS analysis confirmed the formation of the tetrahedron. In Fig. 1a, the inset shows the isotopic pattern for the peak at m/z = 4541.4255, corresponding to $[\mathbf{Eu_4L^4{}_4} + \mathrm{Na}]^+$, which aligns with the calculated values. The lanthanum complex $\mathbf{La_4L^4{}_4}$ is shown in Fig. S9.† To further confirm that the tetrahedron exists as a single species in solution, ^{1}H NMR spectroscopy was employed. Given the low resolution of Eu(III) complexes in ^{1}H NMR, La(III) complexes were used for the NMR experiments. Compared to the free ligand, the result in Fig. 1b reveals that $\mathbf{La_4L^4{}_4}$ exhibits only a single set of signals, indicating the formation of a single species in solution.

In order to determine the structure of the tetrahedral cage $\mathbf{Eu_4L^4{}_4}$, a molecular mechanical model was constructed using the MOPAC 2016 program integrated into the LUMPAC 3.0 software, employing the Sparkle/PM6 approach.[20] Considering the steric hindrance of the ligand, water was selected as the coordinating solvent to satisfy the coordination requirement (8–12) of the lanthanide ions. The optimization results showed that the tetrahedral cage $\mathbf{Eu_4L^4{}_4}$ was synthesized by ligand and lanthanide ions at a stoichiometric ratio of 1 : 1. As shown in Fig. 1c and d, the optimized structure of $\mathbf{Eu_4L^4{}_4}$ is similar to the single crystal structure of $\mathbf{Eu_4L^1{}_4}$. They share similarities in that four Eu(III) ions are chelated with four ligands and located at four vertices of a tetrahedron. Each Eu(III) ion center is coordinated with three β-diketone units in three ligands and two solvent molecules. However, they differ in that the introduced

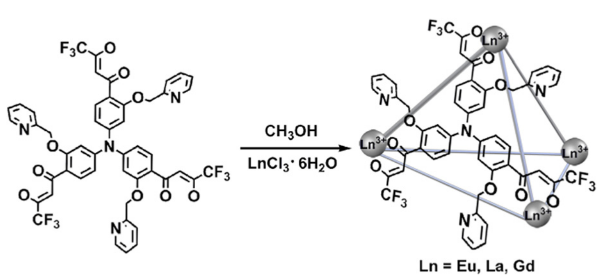

Chart 1 The synthetic method for preparing the lanthanide tetrahedron.

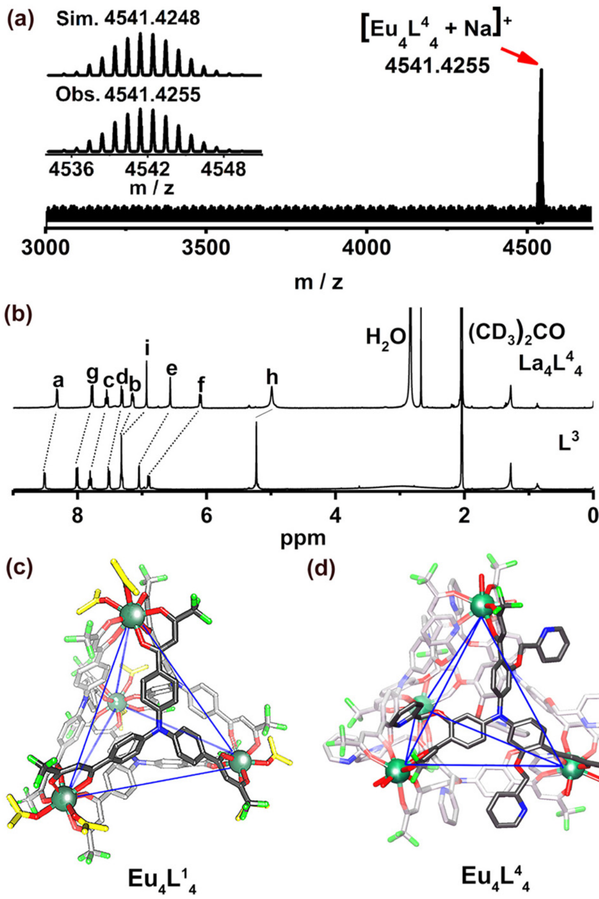

Fig. 1 (a) ESI-TOF-MS spectrum of $\mathbf{Eu_4L^4{}_4}$, with insets displaying the experimental (Obs.) and theoretical (Sim.) isotopic distribution; (b) ^{1}H NMR (400 MHz) spectra of the free ligand $\mathbf{L^4}$ and $\mathbf{La_4L^4{}_4}$ in $(CD_3)_2CO$; (c) crystallographic structures of $\mathbf{Eu_4L^1{}_4}$; and (d) optimized ground-state geometry of $\mathbf{Eu_4L^4{}_4}$.

pyridine group in $\mathbf{Eu_4L^4{}_4}$ is distributed along the three arms of the ligand like a propeller, which increases the interaction between the tetrahedron and the analytes. The cavity volume of the tetrahedral cage is calculated to be 301 Å^3, and the specific cavity size imposes certain limitations on host–guest recognition.

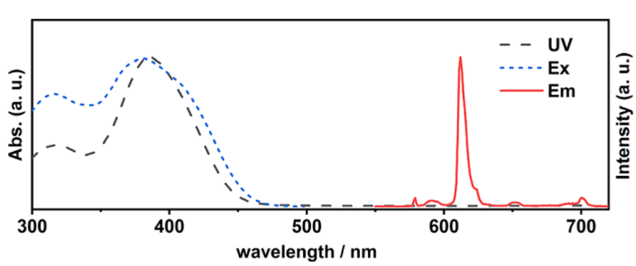

Fig. 2 The graph of emission, excitation and UV-vis absorption spectra of $\mathbf{Eu_4L^4{}_4}$ in THF/CH$_3$CN (v_{THF}/v_{CH_3CN} = 1 : 9, c = 0.25 × 10^{-5} M).

2.2 Photophysical properties of $\mathbf{Eu_4L^4{}_4}$

The photophysical properties of a tetrahydrofuran solution of $\mathbf{Eu_4L^4{}_4}$ (0.25 × 10^{-5} mol L^{-1}) are shown in Fig. 2. The UV-Vis spectrum exhibits two prominent absorption bands, one between 300 and 330 nm and another between 350 and 450 nm. The lower-energy absorption band is attributed to the π–π* charge transfer from the triphenylamine skeleton to the β-diketone unit, while the higher-energy absorption band (300–330 nm) arises from contributions of both the triphenylamine and β-diketone units. When the characteristic emission of the Eu(III) ion at 612 nm is used as the emission wavelength, the excitation spectrum of the complex largely overlaps with the UV absorption spectrum, confirming efficient energy transfer from the ligand to the Eu(III) ions. Upon excitation at 380 nm, the emission spectrum of the $\mathbf{Eu_4L^4{}_4}$ complex in solution reveals a series of sharp transitions corresponding to $^5D_0 \rightarrow {}^7D_J$ (J = 0–4) emissions from the Eu(III) ion, with observed wavelengths at 579, 593, 612, 650, and 702 nm.

2.3 Responses of $\mathbf{Eu_4L^4{}_4}$ to biogenic amine

As shown in Fig. 3a, to explore the sensitivity of the lanthanide tetrahedron $\mathbf{Eu_4L^4{}_4}$ to biogenic amines with different steric hindrance in the solution state, ethylenediamine (EDA),

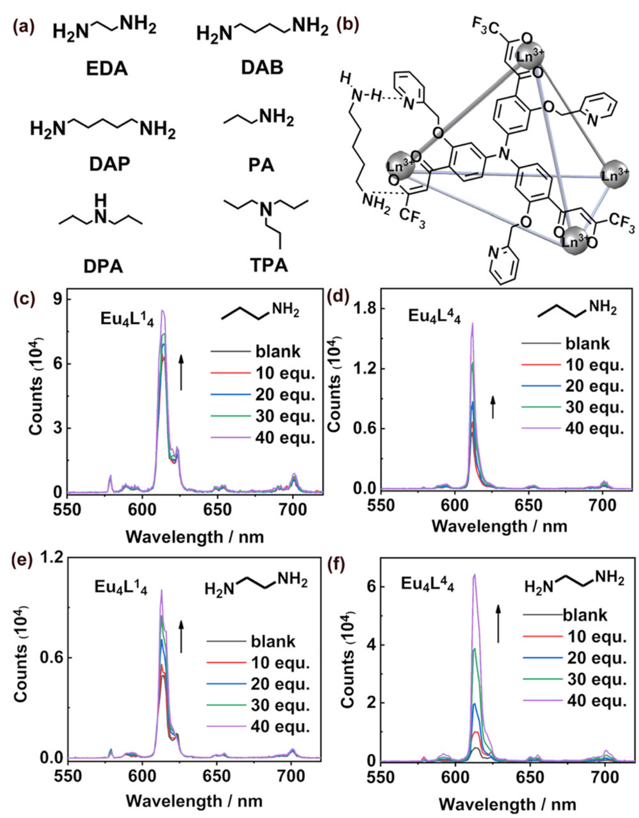

Fig. 3 (a) Biogenic amines studied in this paper; (b) the structure produced by the reaction of $\mathbf{Ln_4L^4{}_4}$ with diamine; (c) emission spectra of $\mathbf{Eu_4L^1{}_4}$ after adding PA; (d) emission spectra of $\mathbf{Eu_4L^4{}_4}$ after adding PA; (e) emission spectra of $\mathbf{Eu_4L^1{}_4}$ after adding EDA; and (f) emission spectra of $\mathbf{Eu_4L^4{}_4}$ after adding EDA (c = 0.25 × 10^{-5} M in THF).

putrescine (DAB), cadaverine (DAP), propylamine (PA), dipropylamine (DPA), and tripropylamine (TPA) were gradually added to a tetrahydrofuran (THF) solution of the Eu(III) complex (concentration: 0.25×10^{-5} mol L^{-1}). The concentration-dependent curve of the luminescence intensity at 612 nm was then recorded. In the solution state, the sensing performance of $\mathbf{Eu_4L^4_4}$ and $\mathbf{Eu_4L^1_4}$ toward monoamines are shown in Fig. 3c and d. It can be observed that as the concentration of various monoamines increases, the luminescence intensity of both complex solutions gradually increases. However, at the same concentration of $\mathbf{Eu_4L^1_4}$ and $\mathbf{Eu_4L^4_4}$ in THF solution, the change in luminescence intensity of $\mathbf{Eu_4L^4_4}$ is significantly more pronounced than that of $\mathbf{Eu_4L^1_4}$ upon the addition of the same concentration of monoamine.

The detection performance of tetrahedral $\mathbf{Eu_4L^4_4}$ and $\mathbf{Eu_4L^1_4}$ for diamines is shown in Fig. 3e and f. Notably, the luminescence intensity of $\mathbf{Eu_4L^4_4}$ increases up to 16 times its initial value when 40 equiv. of EDA are added to the THF solution, whereas the luminescence intensity of $\mathbf{Eu_4L^1_4}$ increases only 3-fold. This demonstrates that $\mathbf{Eu_4L^4_4}$ exhibits significantly better diamine detection performance in solution compared to $\mathbf{Eu_4L^1_4}$. The emission spectral changes for other biogenic amines are shown in Fig. S12.† Additionally, the luminescence lifetimes of $\mathbf{Eu_4L^4_4}$ before and after the addition of DAB were measured. As shown in Fig. S13,† when 12 equiv. of DAB were added, the luminescence lifetime of $\mathbf{Eu_4L^4_4}$ increased to twice its original value. This change in lifetime is consistent with the observed increase in luminescence intensity upon amine addition.

Sensitivity is one of the most essential properties of high-quality sensors; therefore, the lower detection limit has always been a challenge in this field. The limit of detection (LOD) was estimated at a signal-to-noise ratio of 3. The linear relationship between the luminescence intensity of the two cages and the concentration of various amines are shown in Fig. 4 and

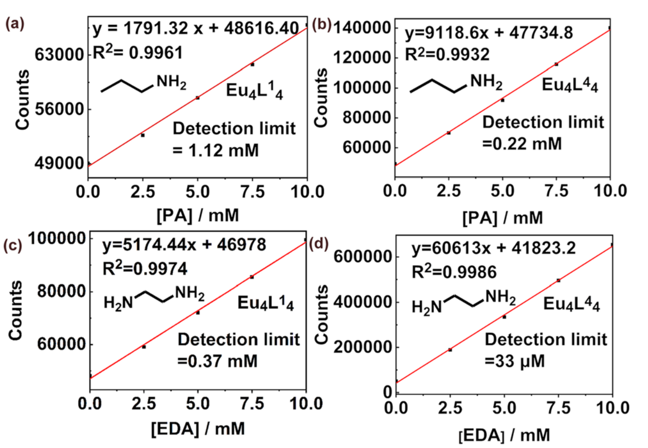

Fig. 4 (a) The variation in luminescence emission of $\mathbf{Eu_4L^1_4}$ upon the addition of PA; (b) the variation in luminescence emission of $\mathbf{Eu_4L^4_4}$ upon the addition of PA; (c) the luminescence emission change of $\mathbf{Eu_4L^1_4}$ with the addition of EDA; (d) the luminescence emission change of $\mathbf{Eu_4L^4_4}$ with the addition of EDA (0 → 10 mM).

Fig. S14,† as well as Tables S1 and S2.† The detection limits of the two tetrahedral cages for various amines range from micromolar to millimolar levels. The low detection limit provides a necessary prerequisite for the detection of biogenic amines by the tetrahedral cage $\mathbf{Eu_4L^4_4}$. As seen in Fig. 4a and b, the detection limit of $\mathbf{Eu_4L^4_4}$ for PA is 0.22 mM, whereas that of $\mathbf{Eu_4L^1_4}$ for propylamine is 1.12 mM. Additionally, $\mathbf{Eu_4L^4_4}$ exhibits slightly lower detection limits for other monoamines compared to $\mathbf{Eu_4L^1_4}$ in tetrahydrofuran solution.

The detection limits of $\mathbf{Eu_4L^4_4}$ and $\mathbf{Eu_4L^1_4}$ for various diamines are shown in Fig. 4c and d. $\mathbf{Eu_4L^4_4}$ (33 μM) has a much lower detection limit for diamines than $\mathbf{Eu_4L^1_4}$ (370 μM). This is due to the fact that $\mathbf{Eu_4L^4_4}$ has two sites, trifluoroacetyl and pyridine, which can both interact with amines, and is more likely to form a ring-like stable structure with diamines than $\mathbf{Eu_4L^1_4}$ with only one site of trifluoroacetyl[21] (as shown in Fig. 3b). Therefore, $\mathbf{Eu_4L^4_4}$ has stronger interaction with diamines than monoamines. This stronger intermolecular interaction results in a lower detection limit for diamines.

To further validate that $\mathbf{Eu_4L^4_4}$ exhibits higher sensitivity towards biogenic amines than $\mathbf{Eu_4L^1_4}$, we employed the following Hill equation (luminescence turn on) to calculate the binding constants.[22]

$$\log \frac{F - F_0}{F_{\max} - F} = n \log[\mathrm{c}] - \log K_\mathrm{d}$$
$$K_\mathrm{a} = 1/K_\mathrm{d}$$

where F_0 and F are luminescence intensities in the absence and presence of biogenic amines, $F_{\max}$ is the luminescence intensity at saturation binding, and [c] is the biogenic amine concentration. K_d is the intercept of the linear regressions, which corresponds to the dissociation constant, and K_a is the binding constant.

Luminescence intensities of $\mathbf{Eu_4L^4_4}$ and $\mathbf{Eu_4L^1_4}$ with biogenic amines at the concentration range of 2.5 mM–10 mM were recorded. The dissociation constants (K_d) were determined by plotting $\log F - F_0/F_{\max} - F$ *versus* log[c]. As shown in Fig. 5, the linear fitting results show that the binding constants of $\mathbf{Eu_4L^4_4}$ for PA and EDA are 0.2820×10^3 M^{-1} and 0.4229×10^3 M^{-1}, respectively, while the binding constants of $\mathbf{Eu_4L^1_4}$ for these two amines are 0.04968×10^3 M^{-1} and 0.07447×10^3 M^{-1}, respectively. $\mathbf{Eu_4L^4_4}$ exhibits significantly higher binding constants for monoamines and diamines compared to $\mathbf{Eu_4L^1_4}$, which is consistent with the calculated detection limits. This indicates that $\mathbf{Eu_4L^4_4}$ has stronger interactions with biogenic amines, demonstrating higher sensitivity than $\mathbf{Eu_4L^1_4}$. The other spectra and binding constants for these amines are shown in the ESI (Fig. S15, S16 and Tables S3, S4†).

Compared with chromatographic detection, the fast response time is a prominent advantage of luminescent sensors. In order to investigate the response time of $\mathbf{Eu_4L^4_4}$ to various amines, the time-dependent luminescence intensity curves were obtained after adding PA and EDA, as shown in Fig. 6a and b. When 40 equiv. of PA and EDA were added, the luminescence intensity of $\mathbf{Eu_4L^4_4}$ increased instantaneously.

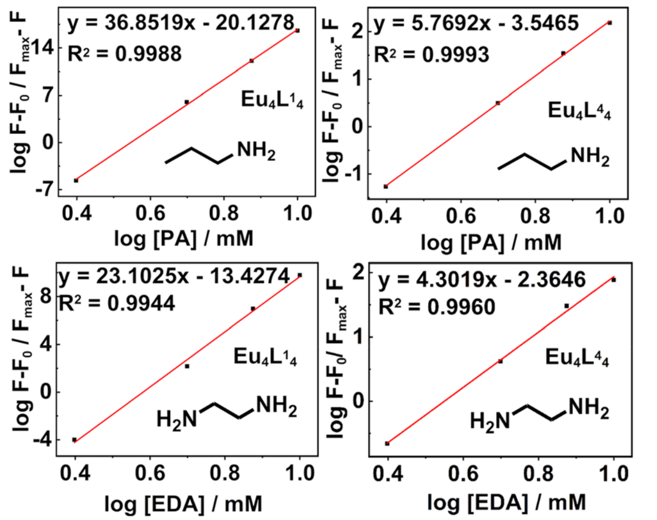

Fig. 5 Linear range of $\log F - F_0/F_{max} - F$ for $\mathbf{Eu_4L^1_4}$ and $\mathbf{Eu_4L^4_4}$ towards log[amine]. The reciprocal of the intercept of the linear regressions is the binding constant of $\mathbf{Eu_4L^1_4}$ and $\mathbf{Eu_4L^4_4}$.

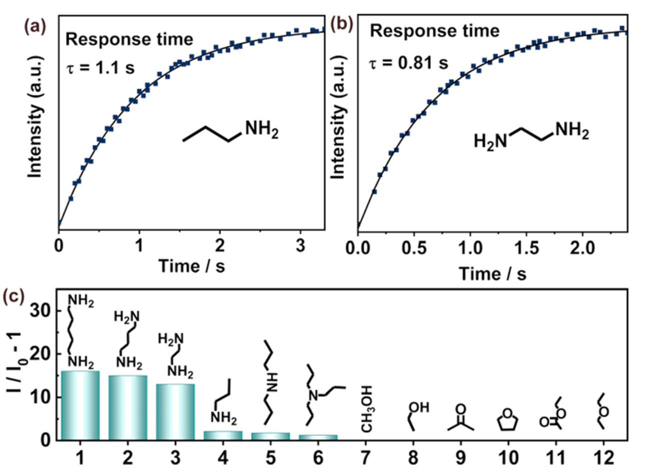

Fig. 6 (a) Response time and time-resolved emission of $\mathbf{Eu_4L^4_4}$ before and after the addition of PA; (b) response time and time-resolved emission of $\mathbf{Eu_4L^4_4}$ before and after the introduction of EDA; and (c) emission changes of $\mathbf{Eu_4L^4_4}$ upon adding various biogenic amines and O-containing compounds.

By fitting the enhancement part of the luminescence intensity enhancement curve, the response times of $\mathbf{Eu_4L^4_4}$ were determined to be 1.1 seconds and 0.81 seconds, respectively. As shown in Fig. S17,† it can be observed that the response times of $\mathbf{Eu_4L^4_4}$ to all biogenic amines are all in the second range, which is far faster than that of any previously reported amine luminescence sensor (Table S5†). Such a fast response time makes $\mathbf{Eu_4L^4_4}$ suitable for real-time monitoring of biogenic amines.

In order to investigate the selectivity of $\mathbf{Eu_4L^4_4}$ to biogenic amines, we selected a series of nucleophilic substances containing oxygen atoms for comparative testing. As shown in Fig. 6c, when 40 equiv. of these nucleophiles were added to the tetrahydrofuran solution of $\mathbf{Eu_4L^4_4}$, the luminescence intensity enhancement ratio $(I/I_0 - 1)$ of $\mathbf{Eu_4L^4_4}$ showed no significant change, with all values remaining below 2%. This result indicates that $\mathbf{Eu_4L^4_4}$ exhibits high specificity for biogenic amines over these nucleophiles.

2.4 Sensing mechanism and luminescence turn on analysis

The interaction mechanism between $\mathbf{Eu_4L^4_4}$ and biogenic amines primarily originates from two aspects: the coordination between biogenic amines and lanthanide ions, or the interaction between amines and ligands in the tetrahedral cage. First, we investigated the intensity ratio of the $^5D_0 \rightarrow {}^7F_2$ to $^5D_0 \rightarrow {}^7F_1$ transitions (I_{F_2}/I_{F_1}), which reflects the symmetry and nature of the Eu(III) ion coordination environment. As shown in Table S6,† the addition of EDA did not induce a significant change in I_{F_2}/I_{F_1}; all the values are around 20, indicating that the introduction of amines did not alter the symmetry around Eu(III). Meanwhile, if amine molecules coordinate to Eu(III), the luminescence intensity of the sensor will decrease due to non-radiative decay. Thus, the possibility of amine coordination to the lanthanide ions can be ruled out.

In order to further explore the interaction mechanism of the lanthanide tetrahedron $\mathbf{Eu_4L^4_4}$ with biogenic amines, the ^{1}H NMR of $\mathbf{Eu_4L^4_4}$ was measured before and after the addition of DAB. The testing procedure is detailed in ESI 1.3.† Due to the paramagnetism of the Eu(III) complex, the resolution of its ^{1}H NMR spectrum is low; $\mathbf{La_4L^4_4}$ was selected as substitution for testing. As shown in Fig. 7, when 12, 24 and 48 equivalents of DAB were titrated into THF-d_8 containing 1 equiv. of $\mathbf{La_4L^4_4}$, all the hydrogen protons in the complex remained observable. Upon the addition of DAB, the signal intensities of all hydrogen protons gradually decreased. The hydrogen proton i on the diketone moiety and the hydrogen protons e, f, and g on the phenyl rings of the triphenylamine shifted slightly upfield. These changes are consistent with the trend observed when

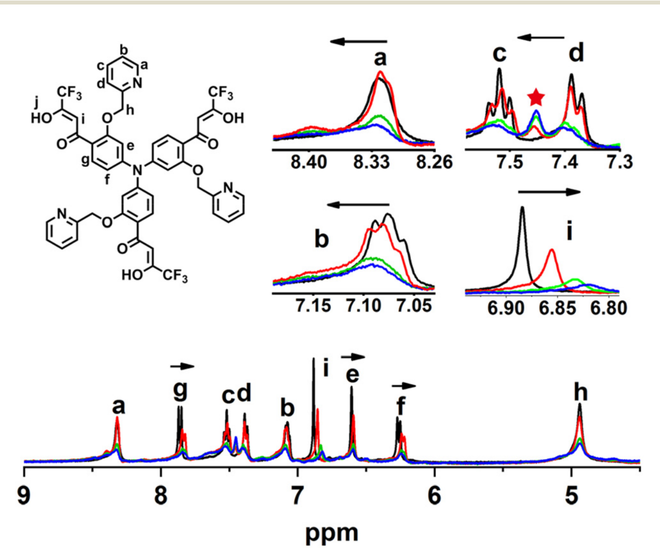

Fig. 7 ^{1}H NMR studies of $\mathbf{La_4L^4_4}$ with the addition of DAB.

$La_4L^1_4$ was treated with amines,[19a] indicating that $La_4L^4_4$, similar to $La_4L^1_4$, can undergo weak intermolecular nucleophilic interactions with biogenic amines. However, the difference is that the hydrogen protons a, b, c, and d on the pyridine ring shifted downfield; generally, hydrogen bonding causes the hydrogen proton to shift downfield. Meanwhile, a new signal peak at 7.45 ppm is obtained, which indicates that there is a stronger intermolecular interaction between $La_4L^4_4$ and DAB compared to nucleophilic interaction. This additional interaction can only be attributed to intermolecular hydrogen bonding between the nitrogen atom on the pyridine ring and the hydrogen atom on the amine.

To further investigate the interaction mechanism between $La_4L^4_4$ and biogenic amines, the NOESY spectrum of $La_4L^4_4$ was tested after adding DAB. The NOE effect requires the distance of adjacent protons to be shorter than 4.5 Å.[23] However, as shown in Fig. S18,† no correlation signals were observed between $La_4L^4_4$ and DAB. Therefore, we can further confirm that no chemical bond was formed between the tetrahedral cage $La_4L^4_4$ and DAB, and the interaction is more likely to involve weak intermolecular nucleophilic interactions and hydrogen bonding. In addition, the 2D-1H-DOSY NMR spectra of $La_4L^4_4$ were examined before and after the addition of DAB. As shown in Fig. S19,† no new diffusion rates were generated; the diffusion rates of both $La_4L^4_4$ and DAB decreased, which may be attributed to their intermolecular nucleophilic interactions and hydrogen bonding interaction leading to a reduction in mobility.

The luminescence quantum yield of Eu(III) complexes mainly depends on the sensitization efficiency of ligands. The alignment between the excited-state energy level and the $^5D_0$ energy level of Eu(III) plays a crucial role in influencing the luminescence intensity of the complex. To explore the reason for the enhanced luminescence intensity of $Eu_4L^4_4$ after the addition of amines, we need to determine the energy levels before and after the addition of amines. The singlet (S_1, $^1\pi\pi^*$) and triplet (T_1, $^3\pi\pi^*$) energy levels of the ligand were calculated using $Gd_4L^4_4$; the UV absorption spectra and phosphorescence spectra of $Gd_4L^4_4$ were examined before and after adding various amines in THF and CH_3CN solution (Fig. S20 and S21†). As shown in Fig. 8a, when 12 equiv. of DAB were added to the acetonitrile solution of $Gd_4L^4_4$, the UV absorption spectrum and phosphorescence emission spectrum exhibited a blue shift, indicating that the singlet and triplet energy levels of the ligand increased after the addition of DAB.

The singlet energy of the ligand is determined by the maximum absorption edge of the UV spectrum of the complex $Gd_4L^4_4$, as shown in Fig. 8b. Upon adding DAB to the solution of $Gd_4L^4_4$, the singlet energy level of the ligand increases from 21 459 cm^{-1} (466 nm) to 22 124 cm^{-1} (451 nm). The triplet energy level of the ligand is calculated based on the lower emission peak wavelength in the phosphorescence spectrum. With the addition of DAB to the $Gd_4L^4_4$ solution, the triplet energy level rises from 19 417 cm^{-1} (515 nm) to 19 881 cm^{-1} (503 nm). Consequently, the energy difference ΔE ($3\pi\pi^* - 5D_0$) between the ligand's triplet state and the excited state of

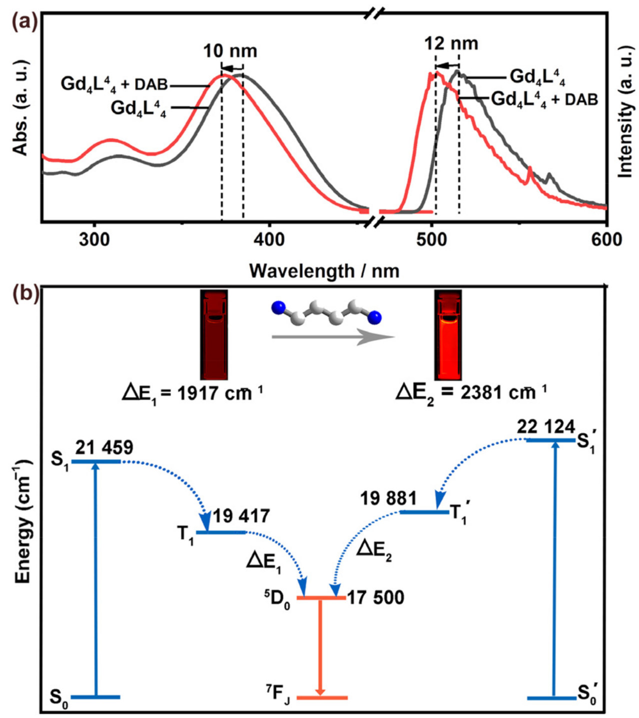

Fig. 8 (a) Phosphorescence and UV/vis absorption spectra of $Gd_4L^4_4$ in THF/CH_3CN before and after DAB addition (v_{THF}/v_{CH_3CN} = 1 : 9, c = 0.25 × 10^{-5} M). (b) Schematic illustration of the energy transfer mechanism for $Gd_4L^4_4$ upon DAB addition.

$Eu_4L^4_4$ increases from 1917 cm^{-1} to 2381 cm^{-1}. For Eu(III) complexes, an optimal energy level difference ΔE is typically between 5000 cm^{-1} and 2500 cm^{-1}. After adding DAB, the energy difference of ΔE = 2381 cm^{-1} is closer to the optimal value of 2500 cm^{-1}. This results in a significant inhibition of energy transfer from the excited state of Eu(III) to the ligand, leading to a noticeable enhancement in the luminescence intensity of $Eu_4L^4_4$.

3. Conclusion

In conclusion, L^4 with multiple reaction sites was synthesized by introducing pyridine groups into the structure of ligand L^1; the tetrahedral cage $Eu_4L^4_4$ was synthesized by coordination-directed self-assembly with lanthanide for the detection of biogenic amines. Combining the comprehensive spectral analyses, an intermolecular weak nucleophilic interaction and a hydrogen-bonding interaction are proposed for this response mechanism. The fitting electrophilic capability of the β-diketonate units to amine nitrogen and hydrogen-bonding interaction endows $Eu_4L^4_4$ with high sensitivity toward biogenic amines. In addition, the confined effect of the tetrahedral cavity could further improve the selectivity of the sensor. Compared with Eu_4L^1, a series of sensing tests showed that the detection limit of $Eu_4L^4_4$ for DAB was reduced from 370 μM ($Eu_4L^1_4$) to 33 μM, and the response time was reduced from 1.1 seconds ($\mathbf{Eu_4L^1{}_4}$) to 0.8 seconds. These results illustrate the effectiveness of increasing the reaction site to improve the sensitivity and selectivity of the sensor, and provide a new strategy for the application of lanthanide sensors in complex organisms.

Author contributions

Yuan Yao: investigation, writing – original draft, data curation, and software. Li Li and Tongxi Zhou: software, formal analysis, and validation. Su Wang and Ying Qin: supervision, data curation, and resources. Chao Fan and Yuying Fu: supervision and writing – review & editing. Guoliang Liu and Hongfeng Li: design, supervision, resources, and writing – review & editing.

Conflicts of interest

The authors declare no competing financial interest.

Data availability

The data that support the findings of this study are available in the ESI† of this article.

Acknowledgements

The authors acknowledge financial support from the Natural Science Foundation of Heilongjiang (No. LH2022B014) and Basic Scientific Research Expenses Project of Provincial Undergraduate Universities of Heilongjiang (No. 2023KYYWF-TD03). We also acknowledge the Sport Molecular Biology Laboratory, College of Sports Science and Health, Harbin Sport University, Harbin 150008, Heilongjiang, People's Republic of China.

References

1 (*a*) B. Prusti, S. Tripathi, A. Jain and M. Chakravarty, Concentration-guided visual detection of multiphase aliphatic biogenic amines through amine-phenol recognition using a dual-state emitter, *ACS Appl. Mater. Interfaces*, 2023, **15**, 16492–16504; (*b*) J. Zou, G. Zhu, X. Lin, L. Chu, H. Zhong, C. Jiang and Y. Huang, Metal-organic frameworks-based nanozyme sensor array for the discrimination of biogenic amines and detection of histamine, *Talanta*, 2025, **284**, 127244; (*c*) S. Yang, J. Du, M. Wei, Y. Huang, Y. Zhang, Y. Wang, J. Li, W. Wei, Y. Qiao, H. Dong and X. Zhang, Colorimetric-photothermal-magnetic three-in-one lateral flow immunoassay for two formats of biogenic amines sensitive and reliable quantification, *Anal. Chim. Acta*, 2023, **1239**, 340660; (*d*) P. C. Wanniarachchi, K. G. U. Kumarasinghe and C. Jayathilake, Recent advancements in chemosensors for the detection of food spoilage, *Food Chem.*, 2024, **436**, 137733.

2 (*a*) B. Dipakkumar and M. Satyendra, Fluorescent-based bile acid triazole-phenothiazine derivatives: Multiphase detection of biogenic amines and application in spoiled foods, *Microchem. J.*, 2024, **207**, 111707; (*b*) M. Katharina, R. Corina and L. M. Schmid, Biogenic amine detection systems for Intelligent packaging concepts: meat and meat products, *Food Rev. Int.*, 2023, **39**, 2543–2567; (*c*) S. Jang, S. U. Son, J. Kim, H. Kim, J. Lim, S. B. Seo, B. Kang, T. Kang, J. Jung, S. Seo and E.-K. Lim, Polydiacetylene-based hydrogel beads as colorimetric sensors for the detection of biogenic amines in spoiled meat, *Food Chem.*, 2023, **403**, 134317; (*d*) C. M. R. Almeida, J. M. C. S. Magalha, M. F. Barroso and L. Durães, Latest advances in sensors for optical detection of relevant amines: insights into lanthanide-based sensors, *J. Mater. Chem. C*, 2022, **10**, 15263–15276.

3 (*a*) Y. Sun, Z. Song, X. Ni, P. Dramou and H. He, A boric acid-functionalized lanthanide metal-organic gel: A ratiometric fluorescence probe with rapid and sensitive detection of dopamine, *Microchem. J.*, 2021, **169**, 106579; (*b*) Y. Yue, F. Huo and C. Yin, Noradrenaline-specific, efficient visualization in brain tissue triggered by unique cascade nucleophilic substitution, *Anal. Chem.*, 2019, **91**, 2255–2259.

4 (*a*) T. Guerrero-Esteban, B. L. Sánchez, L. Expósito, D. Rodríguez-San-Miguel, F. Zamora, F. Pariente, C. Gutiérrez-Sánchez and E. Lorenzo, Synergistic enhancement of electrochemiluminescence through hybridization of α -Ge nanolayers and gold nanoparticles for highly sensitive detection of tyramine, *Sens. Actuators, B*, 2023, **396**, 134649; (*b*) C. L. Devi and B. Martin, highly sensitive electrochemical detection of tyramine using a poly (toluidine blue)-modified carbon screen-printed electrode, *IEEE Sens. J.*, 2022, **22**, 2974–2983; (*c*) W. P. Chathurangi and K. G. Upul, Recent advancements in chemosensors for the detection of food spoilage, *Food Chem.*, 2024, **436**, 137733.

5 S. Mimi, F. D. Ari, D. M. Gordon and V. B. Jill, Measurement of natural variation of neurotransmitter tissue content in red harvester ant brains among different colonies, *Anal. Bioanal. Chem.*, 2020, **412**, 6167–6175.

6 (*a*) C. Yue, A. Lim, M. Chia, P. Wong, J. Chin and W. Wong, Determination of biogenic amines in chicken, beef, and mutton by dansyl chloride microwave derivatization in Malaysia, *J. Food Sci.*, 2023, **88**, 650–665; (*b*) O. O. Akpomie, B. O. Ejechi, A. M. Banach, I. Adewuyi, E. D. Ayobola, K. G. Akpomie, S. Ghosh and S. Ahmadi, Biogenic amine production from processed animal and plant protein-based foods contaminated with *Escherichia coli* and *Enterococcus feacalis*, *J. Food Sci. Technol.*, 2022, **59**, 4880–4888; (*c*) K. Wang, C. Pan, Q. Yang, Q. Ruan, W. Chen, M. Lv, L. Yang, Z. Zou and H. Ma, Detection and quantification of biogenic amines in cephalopod using dansyl chloride pre-column derivatization-HPLC and their production, *J. Food Sci.*, 2024, **89**, 2909–2920.

7 (*a*) F. Čuš, H. B. Česnik and S. V. Bolta, Pesticide residues, copper and biogenic amines in conventional and organic wines, *Food Control*, 2022, **132**, 108534; (*b*) M. Sánchez-Parra, A. Sánchez-Parra, J. L. Ordóñez-Díaz, R. Rodríguez-Solana, J. C. Montenegro-Gómez, J. Pérez-Aparicio and J. M. Moreno-Rojas, Evaluation of biogenic amine and free fatty acid profiles during the manufacturing process of traditional dry-cured tuna, *Food Bioprocess Technol.*, 2024, **17**, 452–463.

8 (*a*) X. Gao, C. Li, R. He, Y. Zhang, B. Wang, Z. Zhang and C. Ho, Research advances on biogenic amines in traditional fermented foods: Emphasis on formation mechanism, detection and control methods, *Food Chem.*, 2023, **405**, 134911; (*b*) Y. Liu, Y. He, H. Li, D. Jia, L. Fu, J. Chen, D. Zhang and Y. Wang, Biogenic amines detection in meat and meat products: the mechanisms, applications, and future trends, *J. Future Foods*, 2024, **4-1**, 21–36.

9 (*a*) J. Hu, Q. Lin, H. Yao, Y. Zhang and T. Wei, Phenazine functionalized pillar [5] arene: Synthesis, host-guest property and application in the fluorescence sensing of biogenic amine in solution, gel and air, *Microchem. J.*, 2023, **194**, 109312; (*b*) G. Meng, C. Zhang, P. Du, S. Sun, X. Zhang, B. Wang and X. Lu, A dual-channel luminescent signal readout nanoprobe for rapid monitoring of biogenic amines in milk and yogurt, *Sens. Actuators, B*, 2022, **357**, 131435; (*c*) L. Cheng, L. Li, P. Sun, H. Zhou, Y. Tian and H. Tang, Synthesis, structure and nonlinear optical properties of two novel two-photon absorption chromophores, *Sci. China, Ser. B:Chem.*, 2009, **52**, 529–534.

10 (*a*) M. L. P. Reddy, V. Divya and K. S. Bejoymohandas, Luminescent lanthanide molecular materials as potential probes for the recognition of toxic and biologically important cations, *Dyes Pigm.*, 2023, **215**, 111248; (*b*) B. Yan, Multiple luminescence responsive chemical sensing of lanthanide functionalized metal-organic frameworks hybrids for logic gate operation application to construct intelligent detecting platform, *Trends Anal. Chem.*, 2024, **170**, 117430; (*c*) X. Wang, Y. Sun, Y. Wang, C. Yu, B. Zhou, J. Zhou, C. Chen, W. Liu and W. Liu, Weak coupling strategy to construct high-performance Sm/Tb-doped lanthanide coordination polymer luminescent sensor for D_2O detection, *Inorg. Chem.*, 2024, **63**, 23680–23690; (*d*) F. Guo, D.-F. Li, F. Gao, K. Xu, J. Zhang, X.-G. Yi, D.-P. Li and Y.-X. Li, Highly Stable Europium(III) Tetrahedral $(Eu_4L_4)(phen)_4$ Cage: Structure, Luminescence Properties, and Cellular Imaging, *Inorg. Chem.*, 2022, **61**, 17089–17100; (*e*) Y. Zhou, H. Li, T. Zhu, T. Gao and P. Yan, A Highly Luminescent Chiral Tetrahedral $Eu_4L_4(L')_4$ Cage: Chirality Induction, Chirality Memory, and Circularly Polarized Luminescence, *J. Am. Chem. Soc.*, 2019, **141**, 19634–19643.

11 (*a*) H. Fu, Z. Xu, Z. Yang and J. Lei, Low-potential anodic electrochemiluminescence of terbium metal-organic frameworks for selective microRNA-155 detection, *Biosens. Bioelectron.*, 2024, **264**, 116675; (*b*) N. Xu, X. Li, F. Luan, C. Tian, Z. Zhang, L. Chen and X. Zhuang, Ratiometric fluorescent and electrochemiluminescent dual modal assay for detection of 2,6-pyridinedicarboxylic acid as an anthrax biomarker, *Anal. Chim. Acta*, 2024, **1288**, 342181; (*c*) M. Zhao, A. Sik, H. Zhang and F. Zhang, Tailored NIR-II lanthanide luminescent nanocrystals for improved biomedical application, *Adv. Opt. Mater.*, 2023, **11**, 2202039.

12 (*a*) C. Ji, J. Zhang, R. Zhang, Y. Chen, Y. Zhang, T. Sun and Y. Yang, A lanthanide-MOF based host–guest intelligent dual-stimulus response platform for naked-eye and ratiometric fluorescence monitoring of food freshness, *J. Mater. Chem. C*, 2023, **11**, 2514–2521; (*b*) L. Guo, D. Zhao, G. Du and H. Li, Fluorescence turn-on mode of Eu^{3+} complex nanocomposite to detect histamine for seafood freshness, *Spectrochim. Acta, Part A*, 2023, **302**, 123089; (*c*) W. Li, Y. Zhou, T. Gao, J. Li, S. Yin, W. Huang, Y. Li, Q. Ma, Z. Yao, P. Yan and H. Li, Circularly Polarized Luminescent $Eu_4(LR)_4$ Cage for Enantiomeric Excess and Concentration Simultaneous Determination of Chiral Diamines, *ACS Appl. Mater. Interfaces*, 2022, **14**, 55979–55988.

13 (*a*) K. Zheng, Z. Liu, Y. Jiang, P. Guo, H. Li, C. Zeng, S. W. Ng and S. Zhong, Ultrahigh luminescence quantum yield lanthanide coordination polymer as a multifunctional sensor, *Dalton Trans.*, 2018, **47**, 17432–17440; (*b*) J. Liu, C. Zhao, J. Yang, Y. Zhou, H. Du, Y. Yang and Y. Yang, A novel hybrid lanthanide metal-organic frameworks based on porphyrin for rapid detection of iron ions, *Anal. Chim. Acta*, 2024, **1319**, 342961.

14 (*a*) S. E. Bodman and S. J. Butler, Advances in anion binding and sensing using luminescent lanthanide complexes, *Chem. Sci.*, 2021, **12**, 2716–2734; (*b*) W. P. Lustig, S. Mukherjee, N. D. Rudd, A. V. Desai, J. Li and S. K. Ghosh, Metal–organic frameworks: functional luminescent and photonic materials for sensing applications, *Chem. Soc. Rev.*, 2017, **46**, 3242–3285.

15 (*a*) A. S. Sharma, M. Marimuthu, A. W. Varghese, J. Wu, J. Xu, X. Luo, S. Devaraj, Y. Lan, H. Li and Q. Chen, A review of biomolecules conjugated lanthanide up-conversion nanoparticles-based fluorescence probes in food safety and quality monitoring applications, *Crit. Rev. Food Sci. Nutr.*, 2024, **64**(18), 6129–6159; (*b*) C. Galaup, C. Picard, F. Couderc, V. Gilard and F. Collin, Luminescent lanthanide complexes for reactive oxygen species biosensing and possible application in Alzheimer'sdiseases, *FEBS J.*, 2022, **289**, 2516–2539.

16 (*a*) Y. Ma, M. Zhu, Y. Zhang, E. Gao and S. Wu, A multiemissive lanthanide metal-organic framework for selective detection of l-tryptophan, *Inorg. Chim. Acta*, 2022, **537**, 120928; (*b*) S. Varghese, J. M. Arya, A. S. Madanan, M. K. Abraham, A. I. Shkhair, G. Indongo, G. Rajeevan, N. S. Vijila, B. K. Arathy and S. George, Highly sensitive lanthanide complex as a probe for L -kynurenine: A cancer biomarker, *Luminescence*, 2024, **39**, e4740.

17 (*a*) H. Ge, Q. Ye, T. Zou, D. Zhang, H. Liu and R. Yang, Recent progress of molecular fluorescent probes with multi-recognition sites enable sensitive and selective analysis, *TrAC, Trends Anal. Chem.*, 2024, **174**, 117685; (*b*) K. Ma, H. Yang, X. Wu, F. Huo, F. Cheng and C. Yin, An

activatable NIR fluorescent probe for NAD(P)H and its application to the real-time monitoring of p53 abnormalities in vivo, *Angew. Chem., Int. Ed.*, 2023, **62**, e202301518; (*c*) Y. Han, L. Mao, Q. Zhang and Y. Tian, Sub-100 ms level ultrafast detection and near-infrared ratiometric fluorescence imaging of norepinephrine in live neurons and brains, *J. Am. Chem. Soc.*, 2023, **145**, 23832–23841.

18 (*a*) H. Yan, Y. Wang, F. Huo and C. Yin, Fast-Specific Fluorescent Probes to Visualize Norepinephrine Signaling Pathways and Its Flux in the Epileptic Mice Brain, *J. Am. Chem. Soc.*, 2023, **145**, 3229–3237; (*b*) N. Zhou, F. Huo, Y. Yue and C. Yin, Specific fluorescent probe based on "protect–deprotect" to visualize the norepinephrine signaling pathway and drug intervention tracers, *J. Am. Chem. Soc.*, 2020, **142**, 17751–17755.

19 (*a*) Y. Yao, Y. Zhou, T. Zhu, T. Gao, H. Li and P. Yan, Eu(III) tetrahedron cage as a luminescent chemosensor for rapidly reversible and turn-On detection of volatile amine/NH_3, *ACS Appl. Mater. Interfaces*, 2020, **12**, 15338–15347; (*b*) Y. Yao, J. Li, Y. Zhou, T. Gao, H. Li and P. Yan, Turn-on luminescence detection of biogenic amine with an Eu(III) tetrahedron cage, *Dyes Pigm.*, 2021, **192**, 109441; (*c*) Y. Yao, C. Zhao, Y. Zhang, G. Cai, F. Wu, J. Sun, X. Liu, T. Zhou, S. Wang, L. Jiang, M. Chen, S. Wang, N. Wu, G. Liu and H. Li, Real time NIR detection of biogenic amine using an Yb_4L_4 tetrahedron, *Opt. Mater.*, 2024, **147**, 114790.

20 J. Dutra, T. D. Bispo and R. O. Freire, LUMPAC Lanthanide luminescence software: efficient and user friendly, *J. Comput. Chem.*, 2014, **35**, 772–775.

21 C. Wang, E. Wu, X. Wu, X. Xu, G. Zhang and L. Pu, Enantioselective Fluorescent Recognition in the Fluorous Phase: Enhanced Reactivity and Expanded Chiral Recognition, *J. Am. Chem. Soc.*, 2015, **137**, 3747–3750.

22 J. Debord, M. Harel, J.-C. Bollinger, L. Koopal, S. Salvestrini and K. H. Chu, Perylene derivatives as a fluorescent probe for sensing of amines in solution, *Dyes Pigm.*, 2016, **134**, 306–314.

23 Z. Dong, G. P. A. Yap and J. M. Fox, Trans -cyclohexane-1,2-diamine is a weak director of absolute helicity in chiral Nickel-Salen complexes, *J. Am. Chem. Soc.*, 2007, **129**, 11850–11853.